Experimental Mechanics
DOI 10.1007/s11340-006-0406-6

Experimental Techniques for the Mechanical Characterization of One-Dimensional Nanostructures

Y. Zhu · C. Ke · H.D. Espinosa

Received: 7 March 2006 / Accepted: 15 September 2006

Abstract New materials and nanostructures with superior electro-mechanical properties are emerging in the development of novel devices. Engineering application of these materials and nanostructures requires accurate mechanical characterization, which in turn requires development of novel experimental techniques. In this paper, we review some of the existing experimental techniques suitable to investigate the mechanics of one-dimensional (1D) nanostructures. Particular emphasis is placed on techniques that allow comparison of quantities measured in the tests with predictions arising from multiscale computer simulations on a one to one basis. We begin with an overview of major challenges in the mechanical characterization of 1D nanostructures, followed by a discussion of two distinct types of experimental techniques: nanoindentation/atomic force microscopy (AFM) and *in-situ* electron microscopy testing. We highlight a recently developed *in-situ* transmission and scanning electron microscopy testing technique, for investigating the mechanics of thin films and 1D nanostructures, based on microelectromechanical systems (MEMS) technology. We finally present the coupled field (electro *and* mechanical) characterization of a NEMS bistable switch *in-situ* a scanning electron microscope (SEM).

Keywords Nanomechanics · *In-situ* microscopy · MEMS · Carbon nanotubes · Nanowires · NEMS

Y. Zhu · C. Ke · H.D. Espinosa (✉, SEM member)
Department of Mechanical Engineering, Northwestern University, 2145 Sheridan Road,
Evaston, IL 60208-3111, USA
e-mail: espinosa@northwestern.edu

Introduction

The discovery of carbon nanotubes (CNTs) by Iijima in the early 1990s sparked an entirely new paradigm for making devices and elicited major fundamental developments within science and technology [1]. Nanowires, nanotubes, and nanobelts of a variety of materials were successfully synthesized and then employed in manufacturing prototype devices in the lab [2, 3]. These nanostructures exhibited not only outstanding mechanical properties [4] but also unique electrical [5], thermal [6] and optical properties [7]. As such, they were envisioned in applications where either material multifunctionality is desirable (e.g., nanocomposites [8]) or in those where new architectures are required to achieve major performance enhancements (e.g., nano-motors [9], nano-switches [10] and nano-sensors [11]). From an engineering viewpoint, electro-mechanical characterization of these nanostructures is essential for the *reliable* design of such devices.

It is well known that strong size dependent mechanical properties arise as the characteristic dimension of the structure approaches or is smaller than 100 nm. This has greatly motivated the mechanics community to investigate nanoscale mechanical behavior from both computational and experimental perspectives. An interesting feature emerging from the mechanics of nanostructures is that they provide an excellent platform for gaining insight into fundamental mechanisms of material deformation and failure. Indeed, the systems contain a limited number of atoms and possible equilibrium configurations, which can be identified in real time by means of *in-situ* X-ray and transmission electron microscopy (TEM). In addition,

because of the limited number of atoms, these systems can be atomistically modeled within the reach of currently available computational power. For instance, CNTs offer a unique system for the study of fracture at the atomic scale because fracture of a single molecule involves only chemical bonds breaking at this scale without other structural complications such as grain boundaries [12]. Likewise, single crystalline metallic nanowires provide the opportunity to investigate dislocation nucleation and their mutual interaction or interaction with surfaces [13]. Therefore, from a scientific viewpoint, direct comparison between nanomechanical tests and atomistic simulations on a one-to-one basis becomes feasible and has the potential to lead to important new discoveries in the context of system reliability.

While theory and simulations are based on somewhat developed theories such as quantum mechanics and molecular mechanics, the experimental techniques used to investigate the mechanics of nanostructures is much less evolved in spite of the fact that some important progress has been made [4, 14, 15]. Moreover, current experimental data are either insufficient or inconsistent, which suggest the need for efforts in developing standardized nanomechanical testing methods.

In this paper, we review recent advances in experimental techniques for nano-mechanical testing, mainly focusing on one-dimensional (1D) nanostructures. We begin by providing an overview of major challenges in the mechanical characterization of 1D nanostructures. Next, we group the available experimental techniques into two categories: nanoindentation/atomic force microscopy (AFM) and *in-situ* electron microscopy testing. We discuss these techniques with special emphasis on specimen fabrication, load/displacement resolutions, and real time imaging capabilities. In particular, we highlight two novel *in-situ* electron microscopy testing techniques recently developed in our lab: a nanoscale material testing system (nMTS) and *in-situ* SEM electromechanical testing of NEMS. Finally, we close the article with concluding remarks and future research directions.

Challenges in the Mechanical Characterization of 1D Nanostructures

Property measurements of 1D nanostructures, such as nanowires and CNTs, are extremely challenging because of their miniscule size. As such, early studies of their mechanical properties focused on theoretical analyses and numerical simulations. Owing to advances in scanning probe and electron microscopies, nanoscale experimental techniques utilizing these tools have been developed. The main challenges in the experimental study of 1D nanostructures include: (1) manufacturing, manipulation and positioning of specimens with nanometer accuracy; (2) application and measurement of forces in the nano-Newton level, and (3) measurement of mechanical deformation with nanometer resolution.

Manipulation and Positioning of Specimens

One of the key steps in nanoscale mechanical testing is the manipulation and positioning, with nanometer resolution and high throughput, of specimens at desired locations. For tensile testing, this becomes even more challenging compared to other types of testing methods, since the specimens must be free-standing and clamped at both ends. Methods for manipulation and positioning of nanostructures are briefly summarized next.

Random dispersion

In this technique, a small aliquot of the 1D nanostructures in suspension is dropped onto a surface containing prefabricated trenches or holes. Statistically, some of the nanostructures are suspended across the gap with random orientation. Typically such configuration is identified by SEM and the end of the nanostructure fixed to the substrate by electron beam induced deposition (EBID) of a gas precursor. Examples are carbon residues present in a scanning electron microscope (SEM) chamber [4], and external precursors such as trimethylcyclopentadienyl-platinum ($(CH_3)_3CH_3C_5H_4Pt$) [15, 16]. Random dispersion has been successfully employed, in combination with atomic probe microscopy, for the bending testing of nanostructures.

Nanomanipulation

Commonly two tools are employed for nanomanipulation: AFMs and multiaxes manipulators. AFM was used to both image and manipulate carbon nanotubes and nanowires. A "NanoManipulator" AFM system, comprising an advanced visual interface for manual control of the AFM tip and tactile presentation of the AFM data, was developed [17]. In addition, Veeco Instruments (Woodbury, New York) developed the "NanoMan" system for high-resolution imaging, high definition nanolithography and direct nanoscale in-plane manipulation.

Electron microscopy provides the imaging capability for manipulating nanostructures with nanometer

resolution. Various nanomanipulators, based on multi-axes piezo actuation, were designed to work inside either SEMs [4, 18] or TEMs [19, 20], see Fig. 1(a). These manipulators are usually composed of both a coarse micrometer-resolution translation stage and a fine nanometer-resolution translation stage, with the latter based on piezo-driven mechanisms capable of subnanometer motions. The manipulators typically have the capability of motion in three linear degrees of freedom, and some possess additional rotational degrees of freedom.

External field alignment

DC and AC/DC electric fields were used for the alignment of nanowires [21], nanotubes [22, 23] and bioparticles [24]. Microfabricated electrodes are typically used to create electric field gradients in the gap between them. A droplet containing nanostructures in suspension is dispensed into the gap with a micropipette. The applied electric field aligns the nanostructures, due to the dielectrophoresis effect, which results in the bridging of the electrodes by a single nanostructure, see Fig. 1(b). Certain electric circuits were used to ensure the manipulation of one single nanostructure [23, 24].

Huang et al. [25] demonstrated another method for aligning nanowires. A laminar flow was employed to achieve preferential orientation of nanowires on chemically patterned surfaces. Magnetic fields have also been used to align carbon nanotubes [26].

Directed self-assembly

Self-assembly is a method of constructing nanostructures by forming stable bonds between organic or non-organic molecules and substrates. Rao et al. [27] reported an approach for large-scale assembly of carbon nanotubes with high-throughput. Dip Pen Nanolithography (DPN) [28], was employed to functionalize the specific surface regions either with polar chemical groups such as amino ($-NH_2/-NH_3^+$) or carboxyl ($-COOH/-COO^-$), or with non-polar groups such as methyl ($-CH_3$). When the substrate with functionalized surfaces was dipped into a liquid suspension containing carbon nanotubes, the nanotubes were attracted towards the polar regions and self-assembled to form pre-designed structures, usually within 10 s, with a yield higher than 90%, see Fig. 1(c). The reported method is scalable to large arrays of nanotube devices by using high-throughput patterning

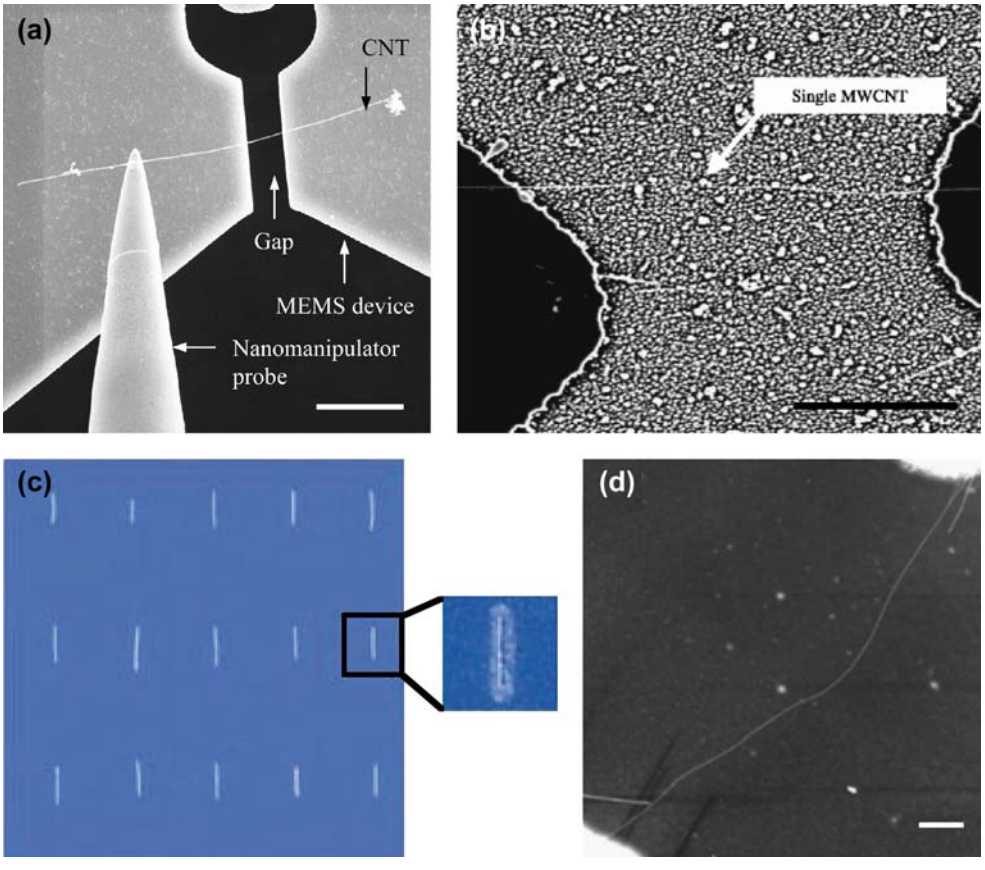

Fig. 1 (**a**) A MWNT across the gap in a freestanding MEMS device by a nanomanipulator (scale bar: 5 μm). (**b**) A MWNT across the gap between two electrodes by electric field alignment (scale bar: 2.73 μm) (Reprinted with permission from [23]. © 2003 Elsevier Ltd.). (**c**) Topography (30×30 μm^2) of an array of individual SWNTs by direct-assembly method. The friction-force image (*inset*) shows a single SWNT (*dark line*), and the regions containing 2-mercaptoimidazole (bright area) and ODT (*dark area*) (Reprinted with permission from [27]. © 2003 Nature Publishing Group). (**d**) A 2-nm diameter individual SWNT bridging two islands by direct growth method. The *bright regions* at the upper right and lower-left corners of the image are the edges of two diagonal islands (scale bar: 500 nm) (Reprinted with permission from [31]. © 1998 Nature Publishing Group)

methods such as photolithography, stamping or massively parallel DPN or nano fountain probes (NFP) [29].

Direct growth

Instead of manipulating and aligning nanostructures after their synthesis, researchers also examined methods for controlled direct growth. Dai and co-workers [30, 31] reported several growth approaches for CNTs. The idea is to pattern a catalyst in an arrayed fashion and control the growth of CNTs between specific catalytic sites, see Fig. 1(d). He et al. [32] recently succeeded in direct growth of Si nanowires between two preexisting single-crystal Si microelectrodes with <111> sidewalls. The catalysts were deposited on the sidewalls of the electrodes and Si epitaxially grown perpendicularly to the <111> surfaces.

Direct growth is a very promising method to prepare specimens for nanomechanical characterization. It does not involve the nano-welding steps used in EBID technique, which brings foreign materials, e.g., carbon and platinum, onto the surface of nanostructures. Such contamination might cause some spurious effects on the properties being measured.

High Resolution Displacement and Force Measurements

Various microscopy techniques such as SEM, TEM and AFM, have been widely used in characterizing nanostructures. These instruments provide effective ways of measuring dimensions and deformation with nanometer resolution. Atomic force microscopy uses a sharp tip at the end of a cantilever, which is driven by a piezoelectric scanner. The instrument resolution is a function of the cantilever stiffness, laser beam optical detection, and software for data reduction. Electron microscopy uses high-energy electron beams for sample imaging through surface scattering (SEM) and volume diffraction (TEM). A field emission gun SEM has a point-to-point resolution of about 1 nm and the TEM is capable of achieving a point-to-point resolution of 0.1~0.2 nm. The resolution of the SEM is limited by the interaction volume between the electron beam and the sample surface; while the resolution of TEM is limited by the spread in energy of the electron beam, and the quality of the microscope optics. The imaging capabilities of these instruments have been used to measure specimen deformation as well as beam deflection and in turn forces.

Commercial force sensors usually cannot reach nano-Newton resolution. Therefore, cantilevers have been effectively employed as force sensors [4, 33], provided that their spring constants have been accurately calibrated. Alternatively, microfabricated frames [14] and microelectromechanical systems (MEMS) [15] offer the capability to measure force with nano-Newton resolution. We will further discuss testing devices and their resolution in the section of "A New MEMS-Based Nanoscale Material Testing System".

Experimental Approaches

Mechanical testing at the nanoscale is rapidly evolving but it remains challenging due to the fact that at least one characteristic dimension of the specimen is only within a few hundred nanometers to a few nanometers. As discussed in the preceding section, specimen fabrication and/or mounting into the testing devices is far from trivial. Likewise, load and displacement measurements with resolutions of nano-Newton (nN) and nano-meter (nm) or better are required.

From a mechanical characterization viewpoint, previously developed experimental techniques can be grouped into two categories: nanoindentation/AFM testing, and *in-situ* electron microscopy testing. Nanoindentation and AFM testing make use of commercially available instruments to apply load and measure deformation simultaneously. Typically, these instruments load the structure in bending mode, although other loading conditions can be achieved, as we will discuss subsequently. *In-situ* SEM and TEM testing require special loading stages that can be placed inside the instruments with the TEM requiring stages only a few millimeters in size. Due to the point-to-point resolution of these field emission instruments, these techniques are probably the most powerful in elucidating deformation mechanisms by real-time imaging of defect nucleation and propagation. Although a variety of techniques have been developed for *in-situ* TEM testing, few achieve *quantitative and simultaneous* load and deformation measurements. In the following subsections, we will review these techniques with a special emphasis on two aspects: 1) fabrication of specimens including effective approaches to manipulate and position specimens onto miniature loading stages; 2) testing mode and associated load and displacement resolutions.

Nanoindentation and Atomic Force Microscopy

A nanoindenter is an instrument that continuously monitors contact load and position. Using feedback control and independent sensing of load and displace-

ment, both load and displacement controlled experiments can be performed. Typically, the instrument load resolution is about 75 nN and the position of the indenter tip can be determined with an accuracy of about 0.1 nm. An AFM is an instrument originally designed to obtain very high-resolution three-dimensional topographical images of surfaces. In an AFM, a sharp tip at the end of a cantilever is brought into contact with the sample surface by moving the tip or sample with piezoelectric-driven scanners. The sample-tip interaction force causes a cantilever deflection, which is typically measured by a laser beam impinging a four quadrant optical detector. Hence, AFM can be readily applied to mechanical testing by applying force to the specimen and measuring deformation. The applied force is computed as the cantilever deflection times the cantilever stiffness. Since deflection can be measured with an accuracy within 0.02 nm, for a typical lever force constant of 10 N/m the force resolution can be as good as 0.2 nN. It is the load and displacement resolution of these two instruments that has been exploited in the nanomechanical characterization of 1D nanostructures. Several experimental configurations were developed requiring the preparation of freestanding samples with the proper boundary conditions and geometric features.

AFM can be operated in several different modes for the mechanical characterization of 1D nanostructures; namely, lateral force mode, contact mode, and force microscopy mode. In the lateral force mode, two methods of sample preparations and loading configurations have been used. In the first method, nanostructures were dispersed randomly on a substrate and some of them were pinned selectively by microfabricated islands [34]. Then AFM was used to bend the cantilevered nanostructures laterally [Fig. 2(a)]. From the measured load-deflection signatures, the elastic modulus, strength and toughness were obtained using continuum mechanics. This technique was applied to multi-walled carbon nanotubes (MWNTs) and silicon carbide nanorods [34]. It is straightforward to implement, however, it cannot eliminate the effect of adhesion and friction from the substrate. To overcome this drawback, in the second method, nanostructures were suspended over a microfabricated trench [35, 36]. The specimens were positioned similarly to the first method except that one additional step consisting of the etching of the substrate under the pinned nanostructure. Another approach consisted in the etching of a trench followed by random dispersion of nanostructures around the trench. After a desirable nanostructure across the trench was identified, EBID of platinum or other materials was employed to clamp it. AFM was used to bend the double-clamped nanostructure laterally, see Fig. 2(b). This technique was used to test single-walled carbon nanotube ropes [35] and gold nanowires [36].

In the contact mode, nanostructures are also clamped at both ends. MWNTs randomly dispersed on an alumina ultrafiltration membrane with 200 nm pores were tested in this fashion. The AFM was used to deflect the suspended nanotubes vertically to obtain load-deflection signatures, see Fig. 2(c). In this example, the adhesion between the nanotubes and the membrane was found sufficiently strong to fix the two ends [33].

The force microscopy technique employs essentially a tensile testing configuration. One end of the specimen is attached to the AFM tip and the other end to a substrate. This technique was applied to measure the quantized plastic deformation of gold nanowires [37]. As shown in Fig. 2(d), both the AFM cantilever and the substrate were coated with a thin layer of gold. A gold nanowire was formed when the AFM cantilever was pressed against the substrate. A piezo-positioner was used to displace the substrate and deform the nanowire in tension. The force was measured from the cantilever deflection and the deformation of the nanowire was determined as the difference between piezo motion and cantilever deflection. This technique has also been effectively employed in understanding the mechanics of single biomolecules, proteins and nanofibers [38–40].

Nanoindentation has been used widely in mechanical characterization of thin films. Recently, it has been extended to testing of 1D nanostructures [41, 42]. The hardness and elastic modulus of silver nanowires were measured using a Hysitron Troboscope nanoindenter [41]. The nanowires were simply dispersed on the substrate. An array of nanoscale indents were successfully made on the wire by direct indention. It was found that the silver nanowire has comparable hardness and elastic modulus to bulk silver [41]. However, since the geometry of indentation of a nanowire differs significantly from that of a half-space, the standard Oliver–Pharr method of analysis is not applicable. Instead, a contact model was developed for the interpretation of nanowire nanoindentation on a flat substrate. Following this new model, Nix and coworkers measured the hardness of GaN and ZnO nanowires [42]. In addition, Waters et al. investigated the shell buckling of individual MWNT using this technique [43]. For the nanoindentation test, the sample preparation is relatively simple; however, the testing requires very careful and precise alignment and positioning of the indenter tip. Moreover, due to the

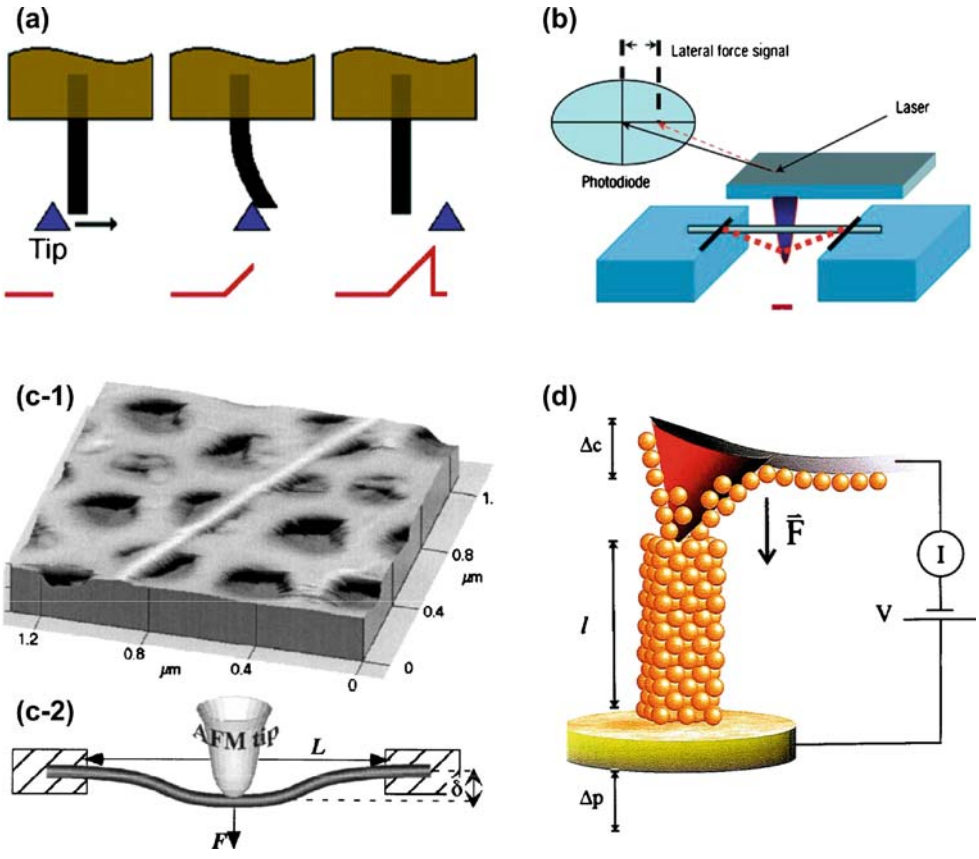

Fig. 2 (**a**) A cantilever nanotube deflected by an AFM in the lateral force mode (Reprinted with permission from [34]. © 1997 American Association for the Advancement of Science). (**b**) A double-clamped nanowire deflected by an AFM in the lateral force mode (Reprinted with permission from [36]. © 2005 Nature Publishing Group). (**c-1**) A MWNT suspended over a porous alumina membrane; (**c-2**) The MWNT deflected vertically by an AFM in contact mode (Reprinted with permission from [33]. ©1999 American Physical Society). (**d**) A gold nanowire stretched by an AFM in force microscopy mode (Reprinted with permission from [37]. © 2000 National Academy of Sciences USA)

comparable size of the indenter tip and the nanowire diameter, the contact model can still be applied for data analysis.

Besides nanoindentation, it is worth mentioning two innovative applications of nanoindenters in mechanical characterization: thin film tension and micro-pillar compression. In the first method, so called membrane deflection experiment (MDE), the nanoindenter load and displacement measurement capabilities were employed to perform *tensile* testing of freestanding thin films by means of a loading configuration and specimen design in which membrane stressing is achieved. The test consists of transversely loading a membrane fixed at both ends and spanning a micromachined window, Fig. 3(a,b). The membrane has a double dog bone shape such that bending effects at the ends and where the load is applied do not control failure [44]. In this configuration a line-load at the center of the span is applied to impose a prescribed deflection history. Simultaneously, an interferometer focused on the bottom side of the membrane records deflection and local deformation. The result is direct tension in the gauged regions of the membrane with load and deflection being measured independently [45]. By means of this technique strong size effects in plasticity and fracture of freestanding polycrystalline face-center cubic (FCC) thin films were identified [46]. The testing methodology was recently extended to study fracture toughness of freestanding thin films [47].

The nanoindenter was also employed in the compression testing of micro-pillars. The pillars were fabricated from a bulk single crystal using FIB [48] or were electroplated [49]. Using the displacement control capability of the nanoindenter, pillars of various sizes were loaded in compression and deformed plastically well into the finite deformation regime, see Fig. 3(c,d) [50]. Stress–strain measurements obtained with this technique and post-mortem SEM observations revealed that when the diameter of the micropillars becomes smaller than a few tens of micrometers, the basic processes of plastic deformation are significantly modified.

Both nanoindenter and AFM techniques were found to possess the capability to record load–displacement histories with high resolution and reliability. In addition, sample preparation is fairly straightforward. However, a major drawback of these techniques is that in general they do not achieve sample imaging while the test is being performed, i.e., observing the sample deformation process while recording load and displacement is not possible. An approach to overcome this limitation is the incorpora-

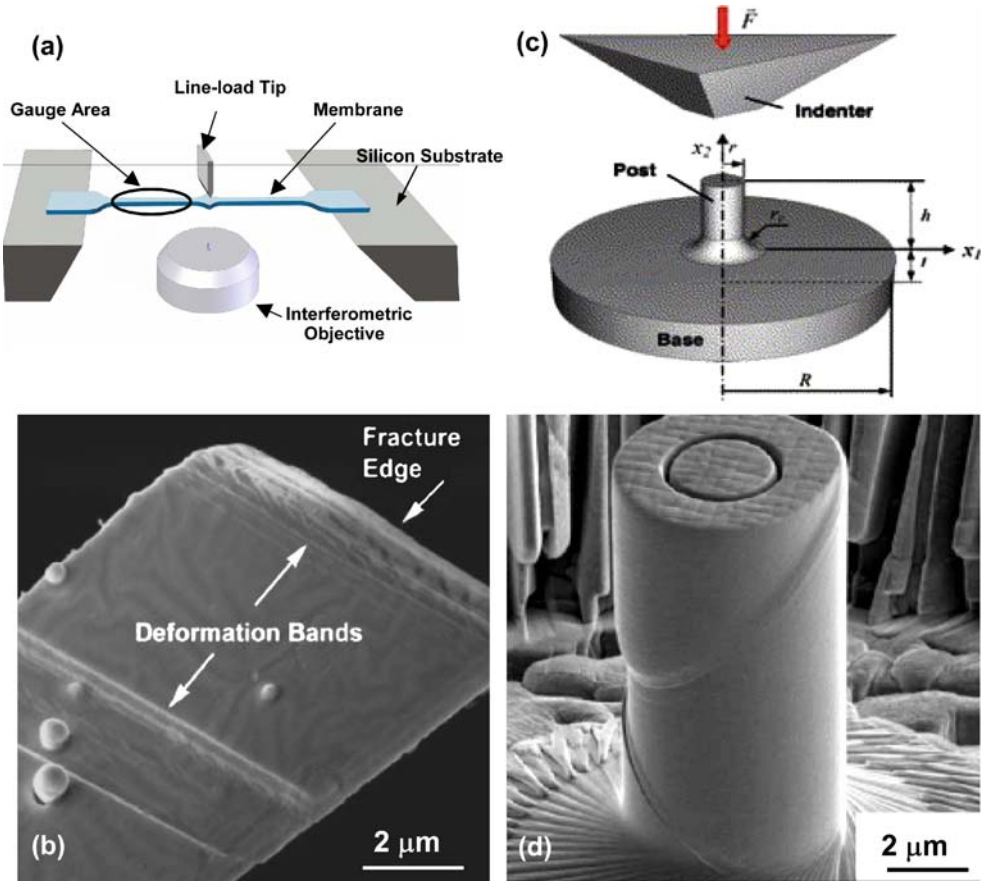

Fig. 3 (**a**) Experimental set-up for MDE testing. (**b**) A typical thin film Au specimen after tested by MDE. Deformation bands and fracture are observed (Reprinted with permission from [63]. © 2005 National Academy of Sciences USA). (**c**) Experimental setup for micro-compression testing of FIB-machined micro-pillar. (**d**) A typical Ni specimen after testing exhibiting multiple slip lines (Reprinted with permission from [49]. © 2005 Elsevier Ltd.)

tion of nanoindenter, AFM or other systems, e.g., MEMS, inside the SEM and TEM.

In-situ Scanning and Transmission Electron Microscopy Testing

In-situ SEM and/or TEM testing allows the usage of high magnifications and in some instances the real time observation of failure initiation. While *in-situ* SEM testing represents a major advance in mechanical characterization at the nanoscale, atomic resolution and real time imaging of defect nucleation and propagation is generally not possible. *In-situ* TEM testing is required for this purpose. Over the years, a large number of *in-situ* TEM studies were pursued on thin film samples [51, 52]; however, the limitation of traditional *in-situ* TEM is its lack of quantitative load and displacement measurement capabilities. As we will discuss below, such capabilities for *in-situ* TEM testing have been recently developed. Resonating the specimen inside the SEM or TEM by means of electrostatic fields is a straightforward technique for mechanical measurements, which has proved to be a useful method for 1D nanostructures [19]. However, it does not provide *in-situ* observation of the specimen deformation history and details about defect initiation and propagation. Therefore, we will not discuss this technique in more detail in this paper.

An example of *in-situ* SEM tensile testing of 1-D nanostructures, mounted by nanomanipulation on a loading system, is the testing of MWNTs, which was performed using double AFM cantilevers in a 5-axes nanomanipulation system based on piezo-actuation [4], see Fig. 4(a). An individual nanotube was clamped to two AFM tips by EBID of carbonaceous material present inside the SEM chamber. A relatively stiff cantilever, connected to one of the piezoactuators, was used to deform the sample while the force was calculated based on the deflection of a soft cantilever. The sample deformation was recorded by SEM imaging. Experiments revealed a "sword-in-sheath" failure mechanism with fracture of the outer shell although direct observation of the shell atomic structure was not possible. Such imaging becomes feasible when the experiment is performed inside a TEM, as we will discuss later.

Co-fabricated thin films attached to a loading frame, containing a beam for load sensing purposes, were

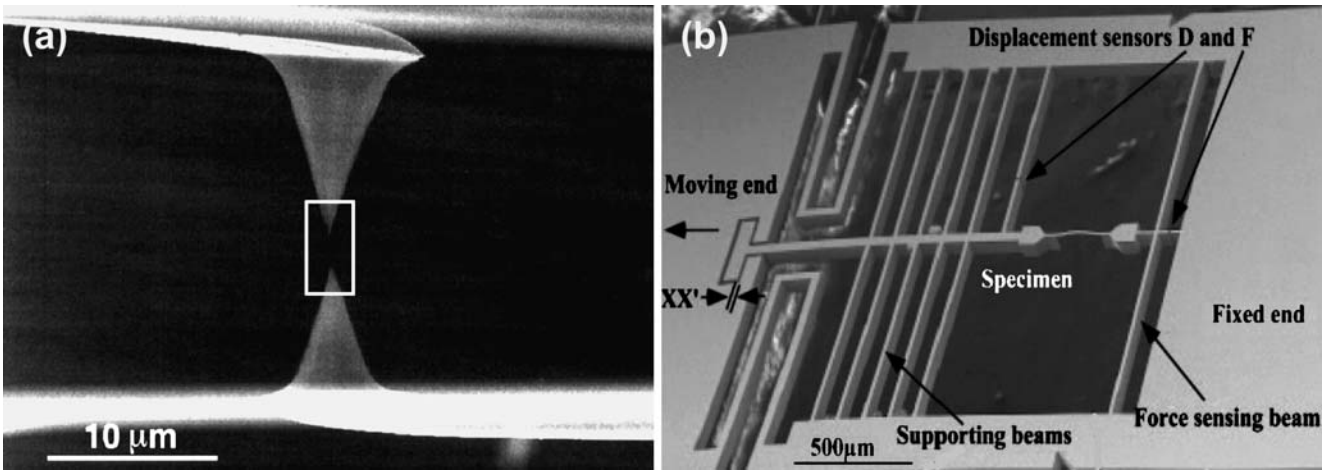

Fig. 4 (**a**) A MWNT mounted between two opposing AFM tips and stretched uniaxially (Reprinted with permission from [4]. © 2000 American Association for the Advancement of Science). (**b**) A microfabricated tensile testing frame including a co-fabricated freestanding thin film and a force sensor (a slender beam). The chip is actuated by an external piezoelectric actuator (Reprinted with permission from [14]. © 2004 National Academy of Sciences USA)

achieved through microfabrication [14], see Fig. 4(b). The loading frame design was such that it could be placed on both SEM and TEM stages. In this configuration, load is applied by external piezo-actuators and monitored by means of beam deflection measurements. As previously mentioned, this load sensing approach prevents simultaneous sample imaging at high magnification, which is needed to identify atomic defect nucleation and propagation. Using this technique, elastic, plastic, and fracture behavior of FCC metals with an average grain size of 50 nm was investigated. Following similar principles, *in-situ* TEM nanoindentation of thin films was achieved [53]. The indenter was mounted on a piezo-actuator but the system did not possess load measurement capabilities. Dislocation nucleation and their interaction with surfaces and other material defects were investigated using this technique [53].

As stated above, one of the most widely employed loading mechanisms inside SEM and TEM instruments is piezo-actuation. This is the case because it can impose deformation with sub-nanometer motion resolution. However, load sensing must be performed independently, which is usually achieved by SEM or TEM imaging of a flexible member attached to the sample in series. A major limitation of this approach is that both sample deformation and load are deduced from the microscopic imaging of the sample and testing apparatus. When high magnifications are employed, these two measurements cannot be made simultaneously. This limitation may be overcome by sensing load without the need of imaging, for instance, electronically [54]. Such a device integrating an actuator and an electronic load sensor has been recently developed by Espinosa and co-workers. Details about its design, resolution and measurements performed with such device are given next.

A New MEMS-Based Nanoscale Material Testing System

We developed a MEMS-based nanoscale material testing system (n-MTS) for *in situ* AFM/SEM/TEM testing of 1D nanostructures. A unique feature of the implemented n-MTS is that it incorporates a capacitive sensor to measure load electronically. This scheme makes possible the *continuous* observation of the specimen deformation and failure, at high magnifications, while independently measuring the applied load. The n-MTS can be used to test 1D nanostructures as well as nanoscale thin films [15, 55].

The n-MTS consists of three parts: actuator, load sensor, and a co-fabricated specimen or gap for placement of a 1D nanostructures, see Fig. 5(a). Two types of actuators were employed in the device design: a comb drive electrostatic actuator and an in-plane thermal actuator. The comb drive actuator achieves force-control while the thermal actuator achieves displacement-control, i.e., it prescribes the specimen displacement as a function of actuator supplied voltage [56].

Details of the principles used in electrostatic and thermal actuation, were described by Kahn et al. [57], Chu et al. [58], and Zhu et al. [56]. The load sensor in the n-MTS consists of a rigid shuttle with one set of

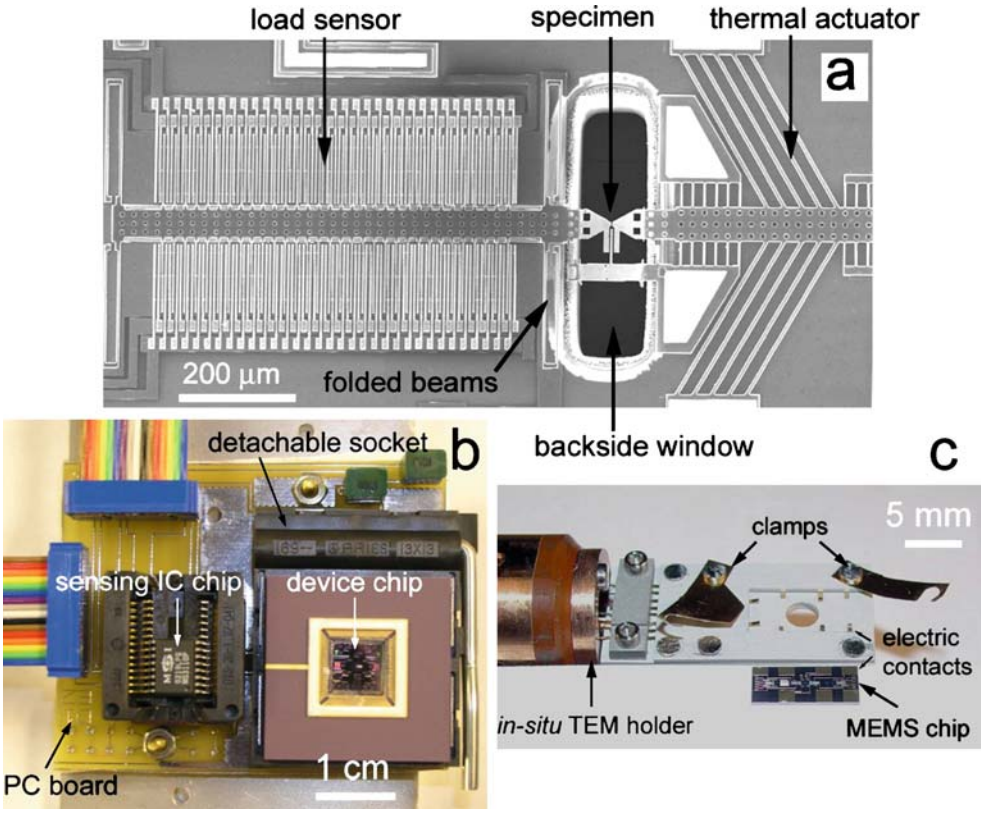

Fig. 5 The n-MTS including actuator, load sensor and specimen. Four folded beams support the load sensor. (**a**) Testing device used in *in-situ* TEM. (**b**) Experimental setup for *in-situ* SEM testing. MEMS device chip is positioned near the MS3110 chip on a printed circuit board. The setup is connected to a power supply, a digital multimeter and a computer outside the SEM by means of a chamber feedthrough. (**c**) *In-situ* TEM holder (containing a feedthrough and eight electric contact pads) along with a 5 mm×10 mm MEMS chip. In an actual experiment, the MEMS chip is flipped, placed in the TEM holder and fixed by the left and right clamps (Reprinted with permission from [15]. © 2005 National Academy of Sciences USA)

movable fingers and two sets of stationary fingers. A lumped model of the sensor consists of two capacitors in series. The displacement of the shuttle causes the increase of one capacitance and the decrease of the other. Within a moderate displacement range, the capacitance change is proportional to the displacement [54]. The load sensor is anchored to the substrate by four folded beams that are designed with a range of stiffness suited for testing various materials of interest (see Espinosa et al. [55] for details).

Measuring capacitance changes with sub-femto-Farad resolution, as required in this application, is quite challenging. We used the so-called charge sensing method to overcome this challenge [59]. A commercially available integrated circuit (IC) based on this method, Universal Capacitive Readout MS3110 (Microsensors, Costa Mesa, CA), was successfully employed. In the SEM implementation of the n-MTS, the MEMS chip was positioned very close to the sensing IC chip (MS3110) in order to minimize stray capacitance and electromagnetic interference. Both chips were placed on a custom-made printed circuit board with grounded shields on both sides [15, 55], see Fig. 5(b). In the TEM implementation, Fig. 5(c), the IC chip us placed outside the TEM holder, which design provides electromagnetic shielding. Characterization of the MEMS actuator and calibration of the load sensor was performed *in-situ* the SEM [15, 54]. We demonstrated the system possesses a displacement resolution of 1 nm, which translates to a load resolution of ~12 nN for a sensor stiffness of 11.8 N/m.

Using this two-chip architecture, nanoscale free-standing polysilicon beams were tested successfully inside the SEM. A dog-bone shaped Poly-Si specimen with a trapezoidal cross-section was obtained by nano-machining using focused ion beam (FIB) (Fig. 6). Two platinum (Pt) lines (with a spacing of 2.5 µm) were deposited by EBID in a dual beam FIB/SEM instrument (FEI, Hillsboro, Oregon) for deformation measurements. Measured stress–strain curves are shown in Fig. 6(c). A Young's modulus of 155±5 GPa and failure strengths of 0.7 GPa and 1.42 GPa, respectively, were identified. Examination of the failure surface, Fig. 6(d), revealed a mirror region at the top right corner of the fracture surface, which is typical of brittle fracture initiation [60–62].

1D nanostructures (NWs and NTs) were also tested inside the SEM. To mount the specimen onto the device, nanomanipulation was performed in a FIB/SEM dual beam instrument [15]. A nanomanipulator possessing 1 nm resolution in three orthogonal directions (Klocke Nanotechnik, Germany) was used to pick up, displace and mount the specimen onto the n-MTS. Figure 7a–d show images corresponding to these

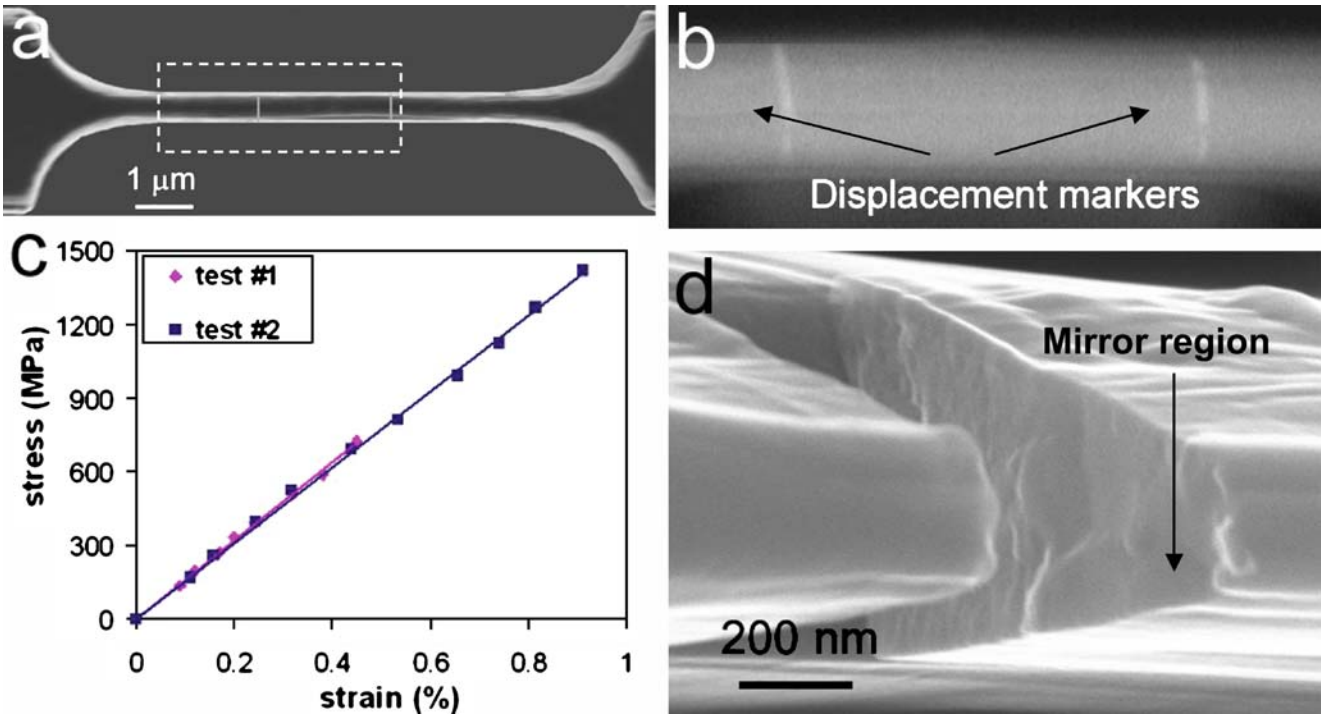

Fig. 6 *In-situ* SEM test of a freestanding polysilicon film. (**a**) Dog-bone shaped tensile test specimen. (**b**) Magnified view of two Pt displacement markers deposited by EBID. (**c**) Stress–strain curves of two *in-situ* SEM tests. Both specimens were 6 μm long and 1.6 μm thick. One had a top width of 0.34 μm and a bottom width of 0.87 μm, while the other had a top width of 0.42 μm and a bottom width of 1.04 μm. (**d**) Fracture surface of polysilicon beam showing a mirror region indicative of brittle fracture initiation (Reprinted with permission from [15]. © 2005 National Academy of Sciences USA)

steps for the case of nanowire. After EBID welding the nanowire to a tungsten tip, connected to the manipulator, the nanowire was brought in contact with the MEMS device (Fig. 7). Contact was confirmed by electron beam and ion beam imaging through two different views. The free end, in contact with the actuator shuttle, was then welded using a Pt precursor and EBID. FIB was then employed to cut the nanowire such that the other end was freed from the nanomanipulator. The manipulator tip was then employed to push down this free end until it made contact with the sensor shuttle. A second Pt nano-weld was then performed. Through this general procedure, several 1D nanostructures were successfully mounted and tested.

The stress–strain curve measured for a Pd nanowire is plotted in Fig. 7(e). The nanowire strain was obtained by measuring the gap between actuator and load sensor shuttles. For this purpose a digital image correlation scheme was used with the shuttle edges used as markers. Assuming that no sliding occurred between the nanowire and the two welded ends, the gap size increase during tensile loading was considered as the nanowire elongation. Hence, strain was computed as the ratio between gap size increase and its initial length (distance between welding points). Examination of Fig. 7(e) reveals a Young's modulus of 99.4±6.6 GPa, which is about 20–30% lower than that of a polycrystalline Pd. Another feature revealed by the test was that the nanowire remained elastic and did not yield nor fracture up to an applied stress of 1.5 GPa. This value is much higher than the yield stress of nanocrystalline Pd in bulk form but smaller than the yield stress predicted by molecular dynamics simulations. This confirms that when the structure size scales down, its strength increases and tends to approach the theoretical strength of the material [63].

We have also tested MWCNTs *in-situ* the SEM and TEM under various electron and ion radiation conditions [55]. The nanotube geometries, radiation conditions and measurement are given in Espinosa et al. [55]. Figure 8(a) is a plot of load-elongation for the tested MWCNTs. The plot shows that as the radiation dose increases, the stiffness of the specimen also increases. The reason for this stiffness increase under tensile loading was inferred from the acquired electron microscopy images. These images revealed that when MWCNTs are subjected to ion beam radiation (high radiation dose), the entire cross section breaks, as shown in Fig. 8(b). By contrast, when MWCNTs are

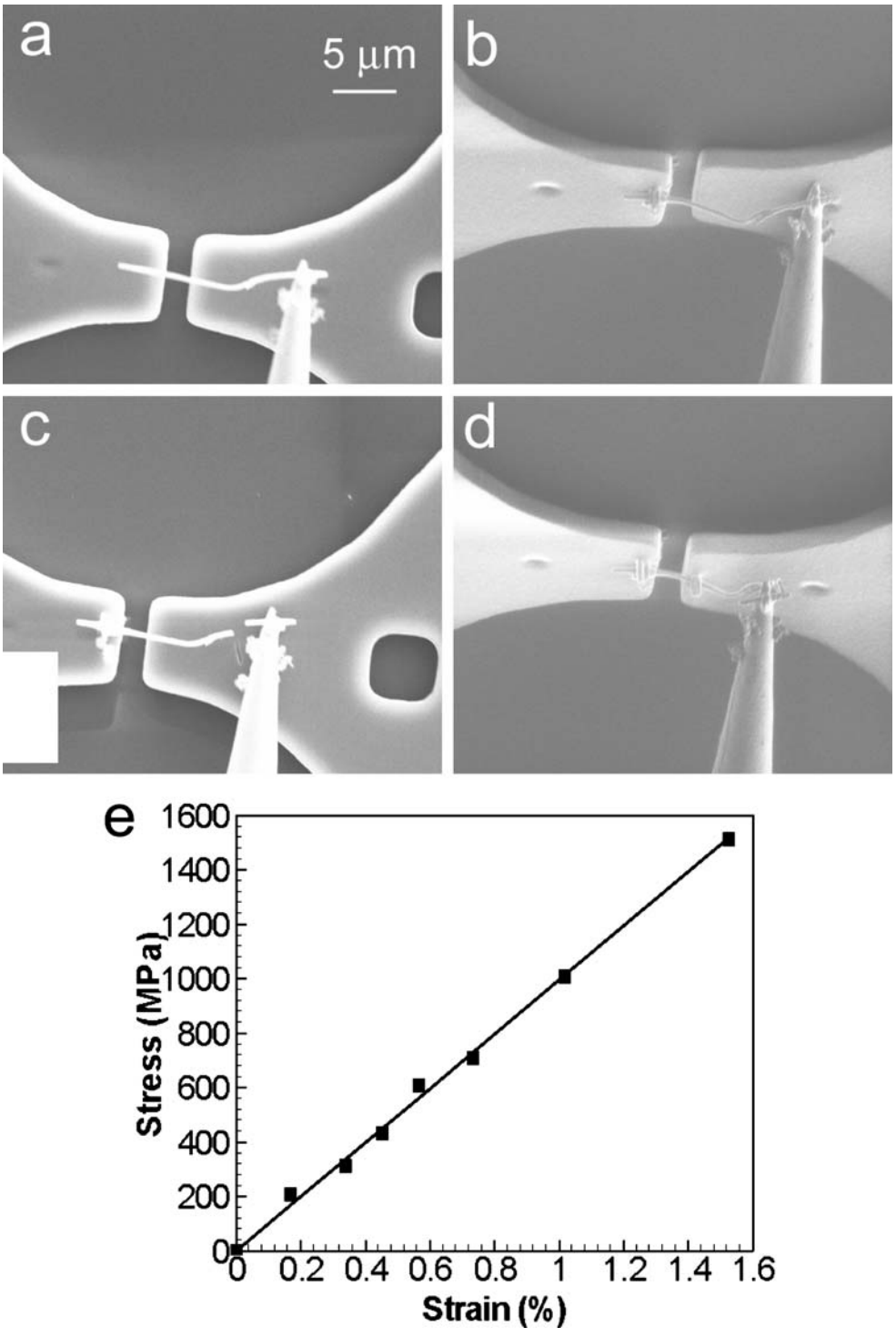

Fig. 7 Images illustrating the nanomanipulation procedure employed to mount a nanowire on a NEMS testing system. (**a**) Approach and contact the nanowire to the MEMS platform. (**b**) Weld one end of the nanowire using EBID of Pt gas. (**c**) Cut the other end using FIB. (**d**) Weld the other end. (**a**) and (**c**) are SEM images, (**b**) and (**d**) are FIB images. There is a 52° view angle difference between SEM and FIB. (**e**) Stress–strain curve of a Pd nanowire exhibiting lower Young's modulus and higher strength than its bulk counterpart (Reprinted with permission from [15]. © 2005 National Academy of Sciences USA)

subjected to e-beam radiation a telescopic failure is observed with the number of outer shell undergoing fracture a function of the radiation dose. Multiple shells fracturing rather than only the outer shell was observed when the experiment was performed *in-situ* the TEM at an operating voltage of 200 kV, see Fig. 8(c). For experiments conducted *in-situ* the SEM at an operating voltage of 5 kV, a single outer shell failure consistent with previously results reported in the literature was observed. This suggests that the electron and ion beam radiation introduces vacancies and crosslinks between the shells. This is corroborated in the literature through experimentation and first principle calculations [64, 65].

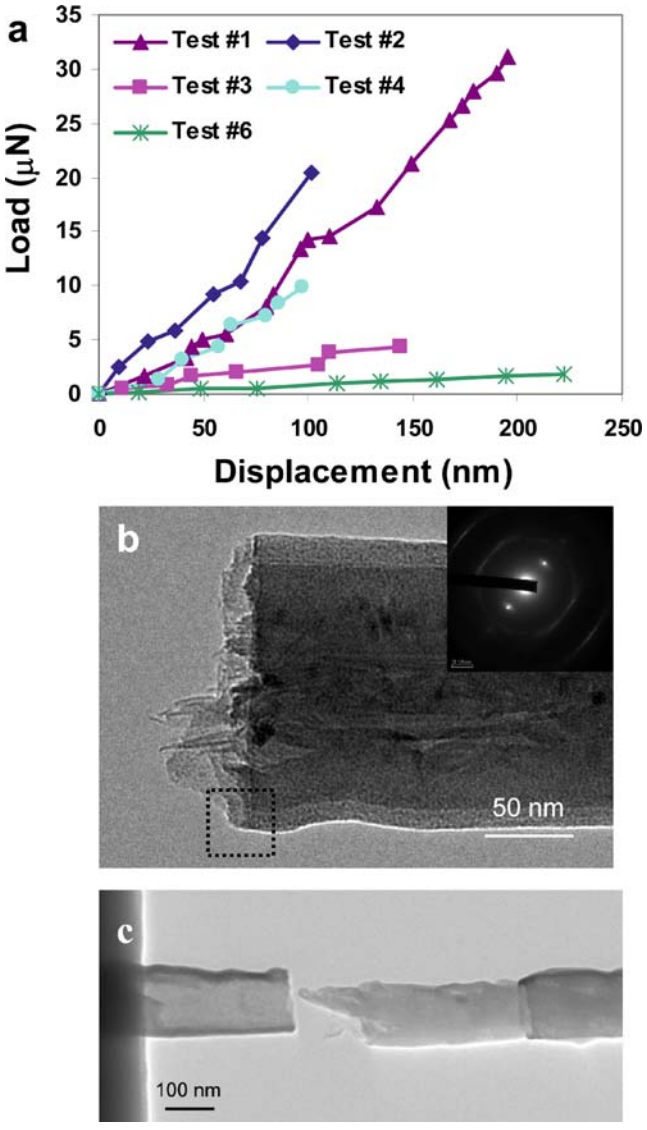

Fig. 8 (**a**) Load-elongation measurements corresponding to CVD-grown MWCNT specimens tested under various irradiation conditions. (**b**) A typical fracture surface of a MWCNT subjected to ion beam irradiation showing failure of the entire cross-sectional area. (**c**) A typical fracture surface of a MWCNT subjected to e-beam irradiation at 200 kV showing telescopic failure with multiple-shells broken (Reprinted with permission from [55]. © 2006 Institute of Electrical and Electronics Engineers)

Another aspect of interest is the stress–strain behavior of the tested nanostructures so we present and discuss them in the sequel. Note that in the process of transforming load–displacement curves into stress–strain curves, the issue of how to define the tube cross sectional area arises. In previous *in-situ* SEM work, when only the outermost shell carries the load, the cross section was defined as $OD \times t$ (where OD is the outer diameter of the MWNT and t is the intershell spacing, about 0.34 nm). However, when crosslinking between multiple shells exists, a new definition for the cross sectional area is needed. For this purpose, we take the *in-situ* SEM measured modulus (based on only one shell failure) as the true modulus of the material and infer the number of failed shells at peak load by matching the calculated Young's modulus. For the CVD grown MWNTs tested in this study, the *in-situ* SEM test revealed a Young's modulus of 315.8±10.8 GPa, which is very similar to the one reported for arc-grown MWCNT. Figure 9 plots the stress–strain curves obtained for the tested MWNTs when subjected to various radiation conditions. The number of shells used in the calculations is reported in the same figure. Failure stresses in the range of 12–20 GPa were measured. Note that these stresses are well below the theoretical stresses predicted for single-walled nanotubes using quantum and molecular mechanics simulations [12]. These authors demonstrate by means of molecular mechanics calculations that defects of a few nanometers in size are needed to explain the measured failure stresses. A distribution of such defects along the tube length would also explain the low modulus experimentally measured.

In-situ SEM Electromechanical Testing of a NEMS Bistable Switch

In addition to the single component testing of CNTs and NWs, testing of these 1D nanostructures as part of a NEMS is also needed. For instance, prototype carbon nanotube based NEMS devices were demonstrated, such as non-volatile random access memory elements (NRAM) [66], nanotweezers [67], tunable oscillator [68], nanorelays [69], and nano-switches [70]. Recently, a cantilever MWCNT-based NEMS device with close-loop feedback control was developed in our lab [10]. In this section and as an example of advances in this area, we will describe such device and present *in-situ* SEM experiments suitable for electromechanical characterization.

The device consists of a conductive nanotube mounted on one electrode (top electrode) as a cantilever freestanding above another electrode (bottom electrode), Fig. 10(a). A resistor and a power supply complete the device circuit. When the applied voltage $U<V_{PI}$ (*pull-in* voltage), the electrostatic field acting on the CNT is balanced by the elastic energy arising from the deformation of the cantilever. The CNT cantilever remains in an "upper" equilibrium position and the deflection is controlled by the applied voltage. Above a certain *pull-in* voltage (the system becomes unstable) and the CNT accelerates towards

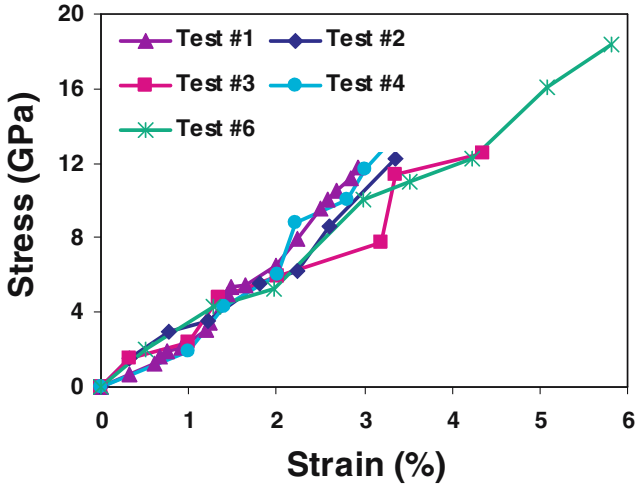

Fig. 9 Stress–strain curves for the tested MWNTs. See text for definition of cross-sectional area (Reprinted with permission from [55]. © 2006 Institute of Electrical and Electronics Engineers)

the bottom electrode. When the tip of the CNT is very close to the bottom electrode (e.g., $\Delta \sim 0.7$ nm), tunneling current flows between the tip-electrode junction. Due to the existence of the resistor R in the circuit, the voltage applied to the CNT drops, weakening the electric field. Because of the accumulated kinetic energy, the CNT continues to move downwards and the tunneling current increases, weakening the electric field further. The elastic force becomes larger than the electrostatic force and the CNT decelerates and changes its direction of motion. Thus the CNT becomes arrested and oscillates around a lower equilibrium position. Due to system damping, the kinetic energy of the CNT is dissipated and the CNT stops in this position with stable current in the circuit. If the applied voltage U decreases, the CNT cantilever starts retracting. When the voltage U decreases beyond a certain value, called *pull-out* voltage, V_{PO}, the CNT cantilever is released from its lower equilibrium position and returns back to its upper equilibrium position. At the same time, the current in the device diminishes substantially. The *pull-in* and *pull-out* processes form a hysteretic loop in voltage–current space, Fig. 10(c). The upper and lower equilibrium positions correspond to "ON" and "OFF" states, respectively. The existence of a tunneling current and the feedback resistor make the "lower" equilibrium state very robust, which is essential to some applica-

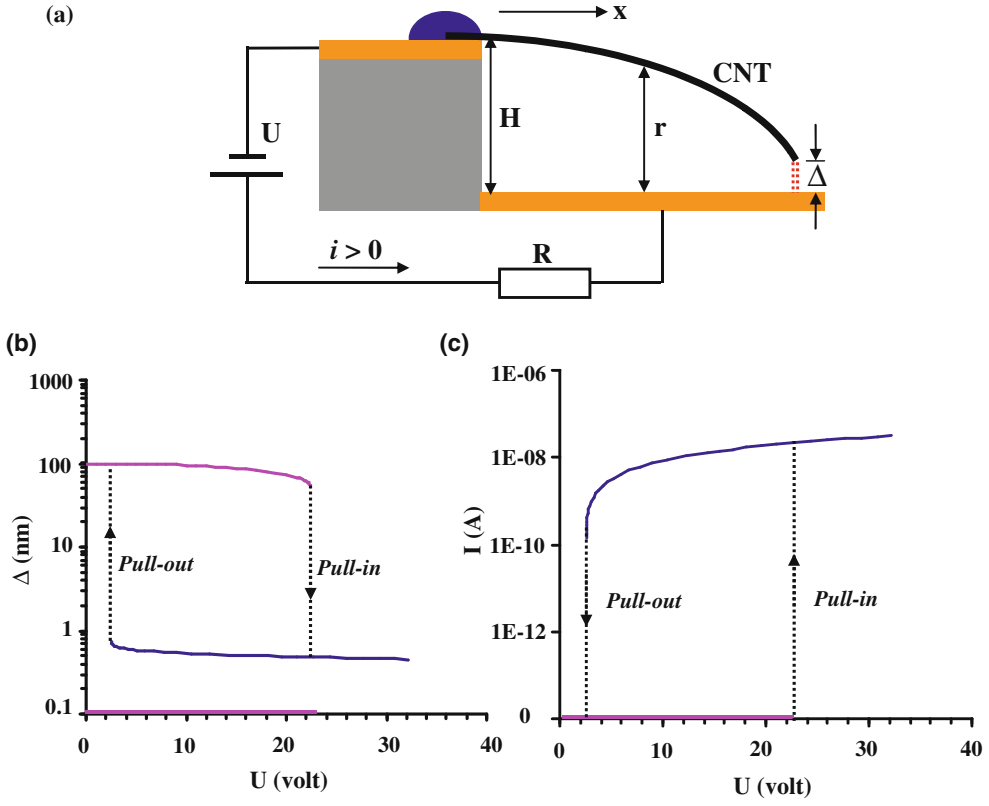

Fig. 10 (**a**) Schematic of feedback controlled CNT based device with tip tunneling. H is the step height and Δ is the gap between the deflected tip and the bottom electrode. Representative characteristic of *pull-in* and *pull-out* processes for the feedback-controlled nanocantilever device: (**b**) Relationship between the gap Δ and the applied voltage U. (**c**) Relationship between the current i in the circuit and the applied voltage U. (Reprinted with permission from [10] © 2004, American Institute of Physics)

tions of interest such as switches, random access memory elements and logic devices. The mathematical modeling of the device was reported in various publications [16, 69, 72].

An important activity in novel NEMS development is the ability to experimentally characterize them. For the case of the bistable switch described above, we pursued this endeavor by performing instrumented *in-situ* SEM experiments. The employed test configuration is schematically shown in Fig. 11(a) [10, 71]. By employing a 3-axes nanomanipulator, Klocke Nanotechnik Co., possessing nanometer positioning accuracy, a multi-wall carbon nanotube was welded to a tungsten probe tip by electron beam induced deposition of platinum. A second electrode employed in the configuration, Fig. 11(a), consisted of a silicon chip coated with a 5-nm-thick Cr adhesion layer and a 50 nm Au film. This chip was glued onto the side of a Teflon block and vertically mounted in the SEM x–y–z stage. The Teflon block with the Au electrode was tilted to meet one of the following testing condition: 1) only the edge could be viewed under the SEM electron beam such that the gap between the nanotube cantilever and the electrode was easily measured; 2) the electrode surface could be viewed so that the electrode surface and the mechanical contact between the nanotube and the electrode could be clearly observed. Using an electric feedthrough, the two electrodes were connected to a resistor R=1 GΩ and to a current–voltage electronic measurement unit (Keithley 4200 SCS). The nanotube cantilever welded to the manipulator probe was displaced until a desired distance (typically 0.5~3 μm, depending on the length and the diameter of nanotubes) between the freestanding CNT and Au electrode was reached. The *pull-in* behavior of the device (gap–voltage curve), in particular, the *pull-in* voltage, and the *pull-in*/*pull-out* behavior of the device (current–voltage curve) were examined systematically using this testing configuration.

Figure 11(b) shows the measured experimental gap–voltage (Δ–U) curve and the theoretical prediction [72–74], for a multiwalled carbon nanotube cantilever 6.8-μm-long and outer diameter of 47 nm placed parallel to the electrode with a gap size of 3 μm [16]. Figure 12(a–e) show the SEM images of the deflection of the carbon nanotube as it was subjected to increasing applied voltages [16]. A feature on the electrode, located in the same horizontal plane containing the cantilever nanotube, is schematically marked as a solid black line in Fig. 12(a–e). Measured deflections and *pull-in* voltage, 48 V, were in good agreement with the theoretical prediction of V_{in}=47.8 V. Figure 11(c) shows an experimentally measured

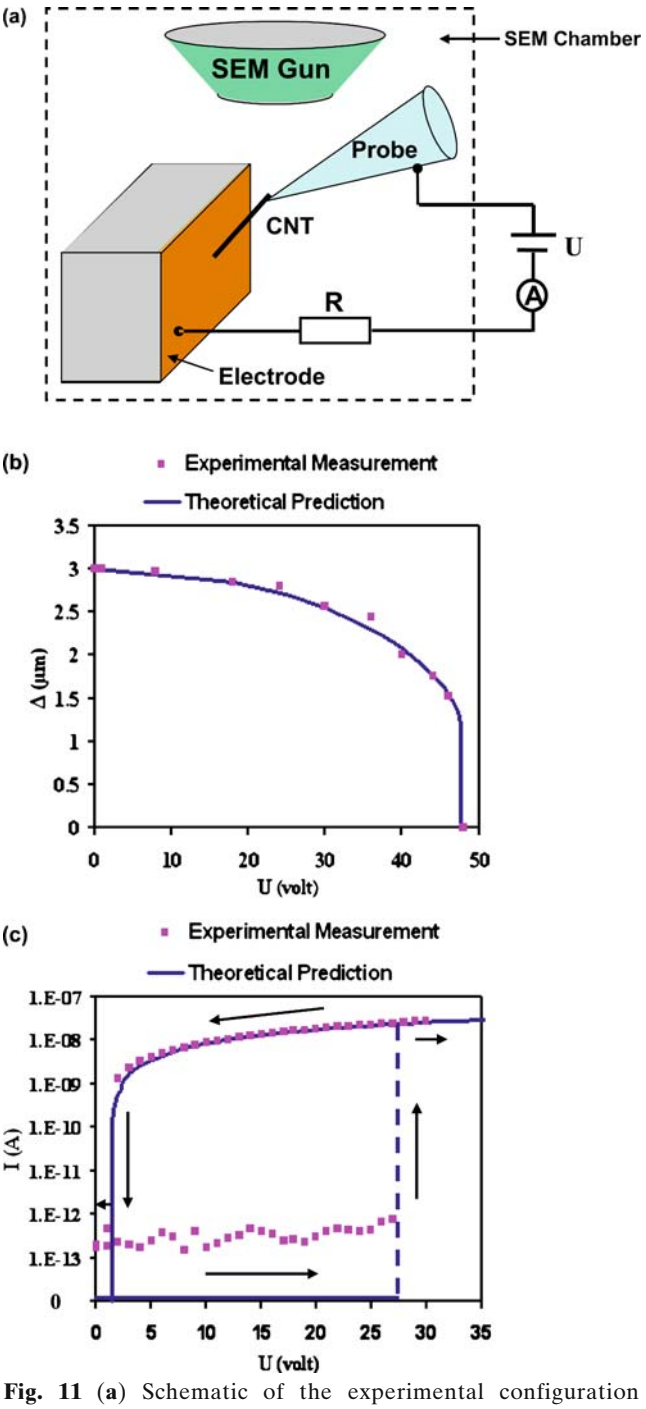

Fig. 11 (**a**) Schematic of the experimental configuration employed for *in-situ* SEM electrostatic actuation of MWNTs. (**b**) Measured Δ–V characteristic curve during pull-in process and comparison with analytical predictions. (Reprinted with permission from [16]. © 2005 Elsevier Ltd.) (**c**) Measured I–V characteristic curve during the *pull-in*/*pull-out* processes and comparison with analytical predictions. The *arrows* show the direction in which the hysteretic loop is described during the increase and decrease of the driving voltage U (Reprinted with permission from [71]. © 2006 WILEY-VCH Verlag GmbH and Co, KGaA Weinheim)

current–voltage (I–U) curve during the *pull-in*/*pull-out* processes and the theoretical prediction for a nanotube

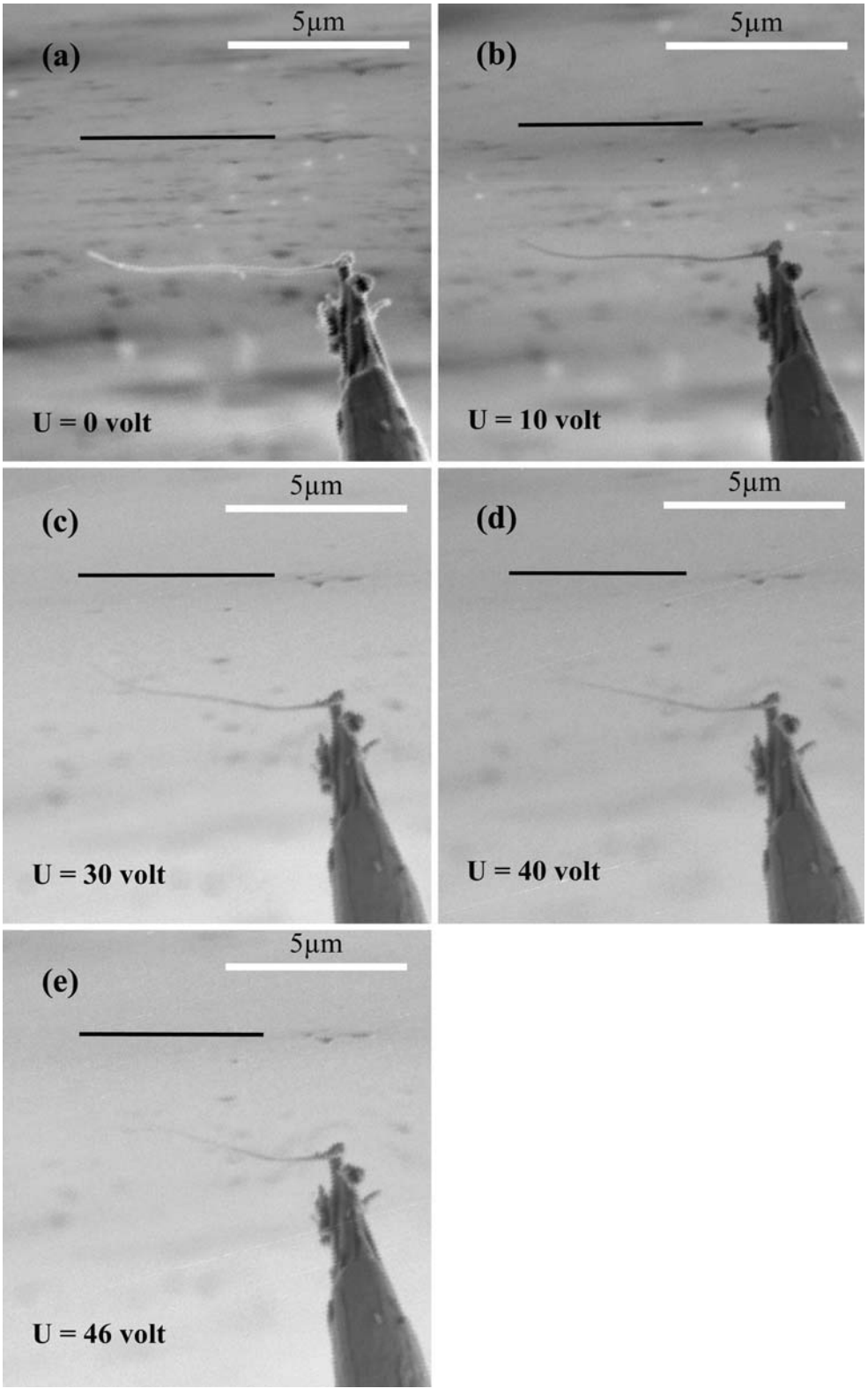

Fig. 12 (**a**–**e**) SEM images of the deformed carbon nanotube at various biased voltages. (Reprinted with permission from [16]. © 2005 Elsevier Ltd.)

9-μm-long [71]. The measured *I–U* curve exhibited the theoretically predicted bi-stability and hysteretic loop. The arrows show the direction in which the hysteretic loop was traveled during the increase and decrease of the driving voltage *U*. The measurement exhibits a background noise of about 0.1 pA, which is typical in these measurements.

It is worth mentioning that the aforementioned *in-situ* electro-mechanical SEM testing methodology is generic and as such it can be advantageously employed to investigate other types of nanotube- or nanowire-based nanoelectromechanical devices.

Concluding Remarks

In this article we reviewed recently developed experimental techniques for the mechanical characterization of 1D nanostructures of particular relevance to emerging MEMS and NEMS technologies. It was highlighted that: 1) a variety of methods have been developed to facilitate the manipulation and positioning of 1D nanostructures; 2) nanoindenter and especially AFM have become indispensable tools for nanomechanical testing due to their extraordinarily high load and displacement resolution; 3) an effort has been made in developing MEMS based testing apparatuses, which can be easily placed inside AFMs, SEMs and TEMs, such that continuous imaging of the specimen can be pursued at high magnifications while electronically and independently measuring load.

Unfortunately, but perhaps not surprisingly, the data from nanomechanical measurements are often contradictory. For example, the Young's modulus of CNTs was reported to be between 0.1 to more than 1 TPa. In this review we have provided some insight into possible sources leading to such inconsistency. Different material fabrication methods may lead to different atomic defect sizes and types. Moreover, different nanomechanical testing techniques, from bending to uniaxial tension configurations with and without real time electron beam imaging, possess a range of resolutions. These findings demonstrate that there is a high need for the development of standardized metrology techniques. In this regard, we have described a novel nanoscale material testing system based on MEMS technology, [15, 54] which may serve as a baseline example. Such approach seems promising and could be extended to a variety of electro-thermal-mechanical characterization configurations. In this regard, a major challenge has been identified, which is the manipulation and positioning of individual nanostructures onto the nanoscale testing systems. The feasibility of this task by mounting and welding individual nanowires and CNTs onto MEMS testing devices was demonstrated [15]. However, the procedure is quite time consuming and gives low yield. Other approaches consisting of direct synthesis of 1D nanostructures on the testing system should be pursued. An example in this direction is the growth of silicon nanowires between two existing electrodes [32]. New synthesis methods should also be investigated to directly synthesize metallic and other nanowires.

While here we have focused on the characterization of mechanical properties, it is recognized that electro-mechanical-thermal characterization is equally important due to the multifunctional features of nanodevices. In this regard, both experimentation and multiscale analysis of the electro-mechanical-thermal behavior under device operational conditions needs to be pursued. Such endeavor is quite challenging but at the same time scientifically stimulating. An example involving the *in-situ* SEM testing of a CNT-based NEMS was demonstrated. Nonetheless, such testing is just in its infancy. Another area that requires particular attention is the scaling up of device nanofabrication to two dimensional arrays. Approaches involving the directed self-assembly of CNTs and NWs seems promising in this respect [32] and should be further investigated.

Finally, key to the future of nanomechanics will be direct comparison between nanomechanical experiments and multiscale simulations of the tested nanostructures. Quantum mechanics and atomistic simulations have been able to predict unique nanomechanical behaviors but they are based on various types of approximations. Hence, the predicted capability of theoretical predictions needs to be assessed by experimentation. With further advances in nanomechanical testing techniques and real time high atomic resolution observations, the source of defects, their nucleation, interaction and evolution will become more quantitative. In turn advances in multiscale modeling will make possible a combined experimental–computational approach clearly required to make further advances in nanoscale material science and its applications.

Acknowledgments The authors acknowledge the support from the FAA through Award No. DTFA03-01-C-00031, ARO through Award No. W911NF-05-1-0088, and the NSF through awards No. CMS-0120866, DMR-0315561. Work was also supported in part by the Nanoscale Science and Engineering Initiative of the National Science Foundation under NSF Award Number EEC-0118025. SEM calibration and testing were performed at the EPIC facility of NUANCE center at Northwestern University. Nanomanipulation was carried out in the Center for Microanalysis of Materials, University of Illinois, which is partially supported by the U.S. Department of Energy

under grant DEFG02-96-ER45439. We thank I. Petrov, J. Mabon and M. Marshall for many useful discussions and for facilitating the microscopy work reported in this manuscript.

References

1. Iijima S (1991) Helical microtubules of graphitic carbon. Nature 354(6348):56–58.
2. Xia YN, Yang PD, Sun YG, Wu YY, Mayers B, Gates B, Yin YD, Kim F, Yan YQ (2003) One-dimensional nanostructures: Synthesis, characterization, and applications. Adv Mater 15(5):353–389.
3. Ke CH, Espinosa HD (2006) Nanoelectromechanical Systems (NEMS) and modeling. Handbook of Theoretical and Computational Nanotechnology. American Scientific Publishers.
4. Yu MF, Lourie O, Dyer MJ, Moloni K, Kelly TF, Ruoff RS (2000) Strength and breaking mechanism of multiwalled carbon nanotubes under tensile load. Science 287(5453):637–640.
5. Wildoer JWG, Venema LC, Rinzler AG, Smalley RE, Dekker C (1998) Electronic structure of atomically resolved carbon nanotubes. Nature 391(6662):59–62.
6. Li DY, Wu YY, Kim P, Shi L, Yang PD, Majumdar A (2003) Thermal conductivity of individual silicon nanowires. Appl Phys Lett 83(14):2934–2936.
7. Duan XF, Huang Y, Agarwal R, Lieber CM (2003) Single-nanowire electrically driven lasers. Nature 421(6920):241–245.
8. Dalton AB, Collins S, Munoz E, Razal JM, Ebron VH, Ferraris JP, Coleman JN, Kim BG, Baughman RH (2003) Super-tough carbon-nanotube fibres — These extraordinary composite fibres can be woven into electronic textiles. Nature 423(6941):703.
9. Fennimore AM, Yuzvinsky TD, Han WQ, Fuhrer MS, Cumings J, Zettl A (2003) Rotational actuators based on carbon nanotubes. Nature 424(6947):408–410.
10. Ke CH, Espinosa HD (2004) Feedback controlled nanocantilever device. Appl Phys Lett 85(4):681–683.
11. Cui Y, Wei QQ, Park HK, Lieber CM (2001) Nanowire nanosensors for highly sensitive and selective detection of biological and chemical species. Science 293(5533):1289–1292.
12. Zhang SL, Mielke SL, Khare R, Troya D, Ruoff RS, Schatz GC, Belytschko T (2005) Mechanics of defects in carbon nanotubes: Atomistic and multiscale simulations. Phys Rev B 71(11).
13. Gall K, Diao JK, Dunn ML (2004) The strength of gold nanowires. Nano Lett 4(12):2431–2436.
14. Haque MA, Saif MTA (2004) Deformation mechanisms in free-standing nanoscale thin films: A quantitative in situ transmission electron microscope study. Proc Natl Acad Sci USA 101(17):6335–6340.
15. Zhu Y, Espinosa HD (2005) An electromechanical material testing system for in situ electron microscopy and applications. Proc Natl Acad Sci USA 102(41):14503–14508.
16. Ke CH, Pugno N, Peng B, Espinosa HD (2005) Experiments and modeling of carbon nanotube-based NEMS devices. J Mech Phys Solids 53(6):1314–1333.
17. Falvo MR, Clary GJ, Taylor RM, Chi V, Brooks FP, Washburn S, Superfine R (1997) Bending and buckling of carbon nanotubes under large strain. Nature 389(6651):582–584.
18. Williams PA, Papadakis SJ, Falvo MR, Patel AM, Sinclair M, Seeger A, Helser A, Taylor RM, Washburn S, Superfine R (2002) Controlled placement of an individual carbon nanotube onto a microelectromechanical structure. Appl Phys Lett 80(14):2574–2576.
19. Poncharal P, Wang ZL, Ugarte D, de Heer WA (1999) Electrostatic deflections and electromechanical resonances of carbon nanotubes. Science 283(5407):1513–1516.
20. Cumings J, Zettl A (2000) Low-friction nanoscale linear bearing realized from multiwall carbon nanotubes. Science 289(5479):602–604.
21. Smith PA, Nordquist CD, Jackson TN, Mayer TS, Martin BR, Mbindyo J, Mallouk TE (2000) Electric-field assisted assembly and alignment of metallic nanowires. Appl Phys Lett 77(9):1399–1401.
22. Chen XQ, Saito T, Yamada H, Matsushige K (2001) Aligning single-wall carbon nanotubes with an alternating-current electric field. Appl Phys Lett 78(23):3714–3716.
23. Chung J, Lee J (2003) Nanoscale gap fabrication and integration of carbon nanotubes by micromachining. Sens Actuators A-Phys 104(3):229–235.
24. Hughes MP, Morgan H (1998) Dielectrophoretic trapping of single sub-micrometre scale bioparticles. J Phys D Appl Phys 31(17):2205–2210.
25. Huang Y, Duan XF, Wei QQ, Lieber CM (2001) Directed assembly of one-dimensional nanostructures into functional networks. Science 291(5504):630–633.
26. Fujiwara M, Oki E, Hamada M, Tanimoto Y, Mukouda I, Shimomura Y (2001) Magnetic orientation and magnetic properties of a single carbon nanotube. J Phys Chem A 105(18):4383–4386.
27. Rao SG, Huang L, Setyawan W, Hong SH (2003) Large-scale assembly of carbon nanotubes. Nature 425(6953):36–37.
28. Piner RD, Zhu J, Xu F, Hong SH, Mirkin CA (1999) "Dip-pen" nanolithography. Science 283(5402):661–663.
29. Kim KH, Moldovan N, Espinosa HD (2005) A nanofountain probe with sub-100 nm molecular writing resolution. Small 1(6):632–635.
30. Dai HJ (2000) Controlling nanotube growth. Physics World 13(6):43–47.
31. Kong J, Soh HT, Cassell AM, Quate CF, Dai HJ (1998) Synthesis of individual single-walled carbon nanotubes on patterned silicon wafers. Nature 395(6705):878–881.
32. He RR, Gao D, Fan R, Hochbaum AI, Carraro C, Maboudian R, Yang PD (2005) Si nanowire bridges in microtrenches: Integration of growth into device fabrication. Adv Mater 17 (17):2098–+.
33. Salvetat JP, Briggs GAD, Bonard JM, Bacsa RR, Kulik AJ, Stockli T, Burnham NA, Forro L (1999) Elastic and shear moduli of single-walled carbon nanotube ropes. Phys Rev Lett 82(5):944–947.
34. Wong EW, Sheehan PE, Lieber CM (1997) Nanobeam mechanics: Elasticity, strength, and toughness of nanorods and nanotubes. Science 277(5334):1971–1975.
35. Walters DA, Ericson LM, Casavant MJ, Liu J, Colbert DT, Smith KA, Smalley RE (1999) Elastic strain of freely suspended single-wall carbon nanotube ropes. Appl Phys Lett 74(25):3803–3805.
36. Wu B, Heidelberg A, Boland JJ (2005) Mechanical properties of ultrahigh-strength gold nanowires. Nat Mat 4(7):525–529.
37. Marszalek PE, Greenleaf WJ, Li HB, Oberhauser AF, Fernandez JM (2000) Atomic force microscopy captures quantized plastic deformation in gold nanowires. Proc Natl Acad Sci USA 97(12):6282–6286.
38. Marszalek PE, Li HB, Oberhauser AF, Fernandez JM (2002) Chair–boat transitions in single polysaccharide molecules observed with force-ramp AFM. Proc Natl Acad Sci USA 99(7):4278–4283.
39. Rief M, Gautel M, Oesterhelt F, Fernandez JM, Gaub HE (1997) Reversible unfolding of individual titin immunoglobulin domains by AFM. Science 276(5315):1109–1112.

40. Tan EPS, Goh CN, Sow CH, Lim CT (2005) Tensile test of a single nanofiber using an atomic force microscope tip. Appl Phys Lett 86(7).
41. Li XD, Hao HS, Murphy CJ, Caswell KK (2003) Nanoindentation of silver nanowires. Nano Lett 3(11):1495–1498.
42. Feng G, Nix WD, Yoon Y, Lee CJ (2006) A study of the mechanical properties of nanowires using nanoindentation. J Appl Phys 99(7).
43. Waters JF, Guduru PR, Jouzi M, Xu JM, Hanlon T, Suresh S (2005) Shell buckling of individual multiwalled carbon nanotubes using nanoindentation. Appl Phys Lett 87(10).
44. Pugno N, Peng B, Espinosa HD (2005) Predictions of strength in MEMS components with defects—A novel experimental–theoretical approach. Int J Solids Struct 42(2):647–661.
45. Espinosa HD, Prorok BC, Fischer M (2003) A methodology for determining mechanical properties of freestanding thin films and MEMS materials. J Mech Phys Solids 51(1):47–67.
46. Espinosa HD, Prorok BC, Peng B (2004) Plasticity size effects in free-standing submicron polycrystalline FCC films subjected to pure tension. J Mech Phys Solids 52(3):667–689.
47. Espinosa HD, Peng B (2005) A new methodology to investigate fracture toughness of freestanding MEMS and advanced materials in thin film form. J Microelectromech Sys 14(1):153–159.
48. Uchic MD, Dimiduk DM, Florando JN, Nix WD (2004) Sample dimensions influence strength and crystal plasticity. Science 305(5686):986–989.
49. Greer JR, Oliver WC, Nix WD (2005) Size dependence of mechanical properties of gold at the micron scale in the absence of strain gradients. Acta Mater 53(6):1821–1830.
50. Zhang H, Schuster BE, Wei Q, Ramesh KT (2006) The design of accurate micro-compression experiments. Scr Mater 54(2):181–186.
51. Cheng S, Spencer JA, Milligan WW (2003) Strength and tension/compression asymmetry in nanostructured and ultrafine-grain metals. Acta Mater 51(15):4505–4518.
52. Legros M, Dehm G, Balk TJ, Arzt E, Bostrom O, Gergaud P, Thomas O, Kaouache B (2003) Material Sciences Society Symposium Proceedings.
53. Minor AM, Morris JW, Stach EA (2001) Quantitative in situ nanoindentation in an electron microscope. Appl Phys Lett 79(11):1625–1627.
54. Zhu Y, Moldovan N, Espinosa HD (2005) A microelectromechanical load sensor for in situ electron and x-ray microscopy tensile testing of nanostructures. Appl Phys Lett 86(1).
55. Espinosa HD, ZhuY, Moldovan N (2005) Design and operation of a MEMS-based material testing system for in-situ electron microscopy testing of nanostructures. Accepted by Journal of Microelectromechanical Systems.
56. Zhu Y, Corigliano A, Espinosa HD (2006) A thermal actuator for nanoscale in-situ microscopy testing: Design and characterization. J Micromech Microeng 16(2):242–253.
57. Kahn H, Ballarini R, Mullen RL, Heuer AH (1999) Electrostatically actuated failure of microfabricated polysilicon fracture mechanics specimens. Proc R Soc Lond A Math Phys Sci 455(1990):3807–3823.
58. Chu LL, Que L, Gianchandani YB (2002) Measurements of material properties using differential capacitive strain sensors. J Microelectromech Sys 11(5):489–498. Kluwer Academic Publisher.
59. Senturia SD (2002) Microsystem design. Kluwer Academic Publisher.
60. Greek S, Ericson F, Johansson S, Furtsch M, Rump A (1999) Mechanical characterization of thick polysilicon films: Young's modulus and fracture strength evaluated with microstructures. J Micromech Microeng 9(3):245–251.
61. Sharpe WN, Jackson KM, Hemker KJ, Xie ZL (2001) Effect of specimen size on Young's modulus and fracture strength of polysilicon. J Microelectromech Sys 10(3):317–326.
62. Tsuchiya T, Tabata O, Sakata J, Taga Y (1998) Specimen size effect of tensile strength of surface-micromachined polycrystalline silicon thin films. J Microelectromech Sys 7(1): 106–113.
63. Espinosa HD, Berbenni S, Panico M, Schwarz KW (2005) An interpretation of size-scale plasticity in geometrically confined systems. Proc Natl Acad Sci USA 102(47):16933–16938.
64. Huhtala M, Krasheninnikov AV, Aittoniemi J, Stuart SJ, Nordlund K, Kaski K (2004) Improved mechanical load transfer between shells of multiwalled carbon nanotubes. Phys Rev B 70(4).
65. Kis A, Csanyi G, Salvetat JP, Lee TN, Couteau E, Kulik AJ, Benoit W, Brugger J, Forro L (2004) Reinforcement of single-walled carbon nanotube bundles by intertube bridging. Nat Mat 3(3):153–157.
66. Rueckes T, Kim K, Joselevich E, Tseng GY, Cheung CL, Lieber CM (2000) Carbon nanotube-based nonvolatile random access memory for molecular computing. Science 289(5476):94–97.
67. Kim P, Lieber CM (1999) Nanotube nanotweezers. Science 286(5447):2148–2150.
68. Sazonova V, Yaish Y, Ustunel H, Roundy D, Arias TA, Mceuen PL (2004) A tunable carbon nanotube electromechanical oscillator. Nature 431(7006):284–287.
69. Kinaret JM, Nord T, Viefers S (2003) A carbon-nanotube-based nanorelay. Appl Phys Lett 82(8):1287–1289.
70. Jang JE, Cha SN, Choi Y, Amaratunga GAJ, Kang DJ, Hasko DG, Jung JE, Kim JM (2005) Nanoelectromechanical switches with vertically aligned carbon nanotubes. Appl Phys Lett 87(16).
71. Ke CH, Espinosa HD (2006) In-situ Electron Microscopy Electro-Mechanical Characterization of a NEMS Bistable Device, Small 2(12):1484–1489.
72. Dequesnes M, Rotkin SV, Aluru NR (2002) Calculation of pull-in voltages for carbon-nanotube-based nanoelectromechanical switches. Nanotechnology 13(1):120–131.
73. Ke CH, Espinosa HD, Pugno N (2005) Numerical analysis of nanotube based NEMS devices—Part II: Role of finite kinematics, stretching and charge concentrations. Trans ASME-J App Mech 72(5):726–731.
74. Ke CH, Espinosa HD (2005) Numerical analysis of nanotube-based NEMS devices—Part I: Electrostatic charge distribution on multiwalled nanotubes. Trans ASME-J App Mech 72(5):721–725.